Acta metall. Vol. 35, No. 7, pp. 1605–1619, 1987
Printed in Great Britain.

0001-6160/87 $3.00 + 0.00

CRACK TIP SHIELDING BY MICRO-CRACKING IN BRITTLE SOLIDS

J. W. HUTCHINSON
Division of Applied Sciences, Harvard University, Cambridge, MA 02138, U.S.A.

(*Received* 22 *October* 1986)

Abstract—The effect of profuse micro-cracking at the tip of a macroscopic crack is studied with emphasis on the reduction in stress intensity, or shielding, within the micro-crack region. Shielding contributions arise from two consequences of micro-cracking, reduction in stiffness and release of residual stress. For the most part the study is limited to the lowest order effect of micro-cracking associated with relatively low micro-crack densities. Shielding results for arbitrarily shaped micro-crack zones are obtained for the case where the orientations of the micro-cracks are randomly distributed. Other possibilities are also discussed and contrasted, and the major uncertainties in quantifying the phenomenon are identified.

Résumé—Nous étudions l'effet d'une microfissuration importante en avant d'une fissure macroscopique, en insistant sur la diminution de la contrainte ou effet d'écran, dans la zone des microfissures. Les contributions à l'écrantage proviennent de deux conséquences de la microfissuration, diminution de la dureté et relâchement des contraintes résiduelles. L'étude est limitée, en majeure partie, à l'effet au premier ordre de la microfissuration associée à des densités relativement faibles de microfissures. Dans le cas d'une distribution aléatoire de l'orientation des microfissures, on obtient un effet d'écrantage pour des zones de microfissures de forme arbitraire. Nous discutons également d'autres possibilités en soulignant leurs différences, et nous identifions les incertitudes majeures de la quantification du phénomène.

Zusammenfassung—Der Einfluß ausgiebiger Mikrorißbildung an der Spitze eines Makrorisses wird im Hinblick auf die Verringerung der Spannungsintensität (Abschirmung) innerhalb des Bereiches der Mikrorisse untersucht. Beiträge zur Abschirmung kommen von zwei Konsequenzen der Mikroriß-Bildung, die Verringerung der Steifigkeit und die Absenkung von Restspannungen. Der überwiegende Teil der Untersuchung ist auf den Effekt kleinster Ordnung der Rißbildung, der mit einer vergleichsweise kleinen Dichte an Mikrorissen zusammenhängt, beschränkt. Ergebnisse zur Abschirmung beliebig geformter Mikroriß-Zonen werden für den Fall zufällig verteilter Mikroriß-Orientierungen erhalten. Andere Möglichkeiten werden ebenfalls diskutiert und gegenübergestellt. Die wesentlichen Unsicherheiten bei der Quantifizierung dieser Erscheinung werden angegeben.

1. INTRODUCTION

There is growing evidence [1–8] that micro-cracking in regions of high stress concentration or at the tip of a macroscopic crack may postpone the onset of unstable macroscopic crack propagation in brittle solids such as ceramics and rocks. For this mechanism to operate it is essential that the micro-cracks arrest at grain boundaries or particle interfaces and be highly stable in the arrested configuration. Ultimately the macroscopic crack advances by interaction and coalescence of the micro-cracks. But the micro-crack zone can also have a shielding effect on the macroscopic crack tip, redistributing and reducing the average near-tip stresses. This shielding process is studied in the present paper in much the spirit as in some earlier studies [4–8]. The discussion in [6] provides a background for the work carried out here.

There are two sources of the redistribution of stresses in the near-tip stress field of the macroscopic crack. One is due to the reduction in the effective elastic moduli resulting from micro-cracking. The other is the strain arising from the release of residual stresses when micro-cracks are formed. The residual stresses in question develop in the fabrication of polycrystalline or multi-phase materials due to thermal mismatches between phases or thermal anisotropies of the single crystals. The spatial variation of these stresses is set by the grain size or by the scale of second phase particles. These residual stresses play an important role in determining the onset and extent of micro-cracking. Moreover, the micro-cracks partly relieve the residual stresses producing strains which are manifest on the macroscopic scale as inelastic, or transformation, strains.

A continuum approach is adopted in this paper in which it is assumed that a typical material element contains a cloud of micro-cracks. The stress–strain behavior of the element is obtained as an average over many micro-cracks. The paper begins with a consideration of two prototype micro-cracking situations from which constitutive behavior is derived. A characteristic tensile stress–strain curve is shown in Fig. 1. The Young's modulus E of the uncracked material governs for stresses below σ_c where micro-cracking first sets in. In this paper, as in most other

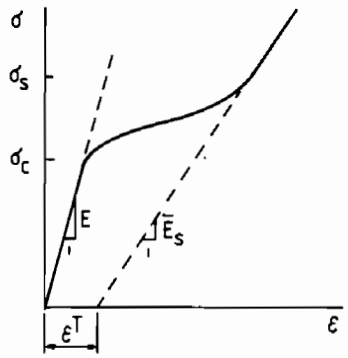

Fig. 1. Characteristic tensile stress–strain curve.

studies to date, it will be assumed that micro-cracking ceases, or saturates, above some stress σ_s. The assumption of the existence of a saturated state of micro-cracking is fairly essential to the analysis carried out here, as will become evident. A strictly saturated state, independent of applied stress, is probably unrealistic. However, it does seem reasonable to expect that the sites for nucleation of micro-cracks will tend to become exhausted above some applied stress level when local residual stresses are playing a central role in the micro-cracking process. Thus, it is tacitly assumed that there exists a zone of nominally constant reduced moduli surrounding an even smaller fracture process zone within which the micro-cracks ultimately link up. A reduced modulus $\bar{E}_s$ governs incremental behavior for stresses above σ_s. The offset of this branch of the stress–strain curve with the strain axis, ϵ^T, is the contribution from micro-cracking due to release of the local residual stresses. It can be thought of as a transformation strain.

Two of the most important assumptions involved in the formulation of the constitutive law deal with the distribution of the orientations of the micro-cracks, whether the reduced moduli are isotropic or anisotropic for example, and the stress conditions for the nucleation of the micro-cracks. Recent microscopic observation of a zirconia toughened alumina [3] suggest that the micro-cracks which form in this system have a more-or-less random orientation with no preferred orientation relative to the applied stress. This would be consistent with the random nature of the residual stresses expected for this system. Nevertheless, there is not yet nearly enough observational information or theoretical insight to justify any one constitutive assumption. The approach taken in this paper has been to consider a number of reasonable alternatives, including some possibilities considered by others. In this way, it is hoped that the results discussed here will serve to bracket actual behavior and give some indication of which uncertainties are most crucial to further development of the subject.

A preview of the type of mechanics problem analysed in this paper is shown in Fig. 2. In this particular problem the micro-crack region, A_c, surrounding the crack tip has reduced moduli which are uniform and isotropic. A uniform transformational dilatation θ^T is also present associated with the release of residual stress. The crack is semi-infinite with a remote stress field specified by the "applied" stress intensity factor K, modeling a finite length crack under small scale micro-cracking conditions. The near-tip fields have the same classical form but their stress intensity factor, K_{tip}, is different. It is the ratio K_{tip}/K which is sought as a function of the moduli differences, θ^T and the shape of the zone. The extent to which K_{tip} is reduced below K reflects the shielding. However, knowledge of K_{tip}/K is not sufficient to predict the toughening increment due to shielding. One also needs to know the inherent toughness of the micro-cracked material compared to similar material which does not undergo this same kind of stress induced micro-cracking. One way or another, K^c_{tip} must be determined or inferred from experiments. Even without hard data on K^c_{tip}, knowledge of K_{tip}/K for different situations, such as stationary or growing cracks, can be used to make comparative assessments of macro-cracking behavior and to gain insight into phenomena such as stable crack growth.

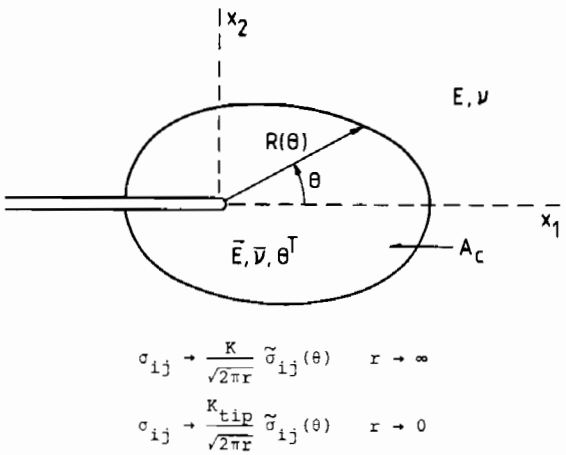

Fig. 2. Geometry of the zone of micro-cracking.

2. REDUCTION IN MODULI AND RELEASE OF RESIDUAL STRESS FOR SOME PROTOTYPE MICRO-CRACKS

The following two examples are chosen to illustrate the way micro-cracking can reduce the moduli of a brittle material and give rise to "inelastic" strain by release of residual stress. Other possibilities can be accommodated in the development of later sections.

2.1. Penny-shaped micro-cracks in a prestressed spherical particle

Consider the configuration indicated in Fig. 3 where an isolated spherical particle or grain of radius b is embedded in an infinite matrix. Both particle and

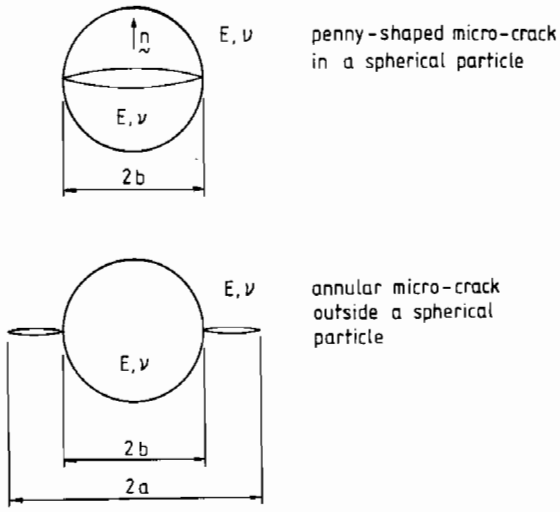

Fig. 3. Two prototypical micro-crack geometries.

matrix are assumed isotropic with common Young's modulus E and Poisson's ratio ν. Suppose the particle sustains a uniform residual stress prior to cracking. Let σ_R denote the normal component (assumed positive) acting across the plane where the micro-crack will form and suppose there is zero tangential traction on this plane. Now suppose a penny-shaped micro-crack is nucleated which arrests at the interface of the particle and the matrix as shown in Fig. 3. The volume of the opened micro-crack is

$$\Delta v = \tfrac{16}{3} b^3 (1-\nu^2) \frac{\sigma_R}{E}. \tag{2.1}$$

The release of the residual stress creates an "inelastic" strain contribution. If the micro-crack forms within a material element of volume V and if interaction with other micro-cracks is ignored, the inelastic strain contribution is

$$\Delta\epsilon_{ij} = \frac{\Delta v}{V} n_i n_j = \frac{16}{3}\frac{b^3}{V}(1-\nu^2)\frac{\sigma_R}{E} n_i n_j \tag{2.2}$$

where n_i is the unit normal to the plane of the micro-crack. This is a uniaxial strain contribution with dilatational component

$$\Delta\epsilon_{kk} = \frac{16}{3}\frac{b^3}{V}(1-\nu^2)\frac{\sigma_R}{E}. \tag{2.3}$$

The formation of the micro-crack also increases the compliance of the material element [9]. With σ_{ij} as the macroscopic stress experienced by the material element, the increase in strain due to a component of stress acting normal to the plane of the micro-crack (i.e. $\sigma_{nn} = \sigma_{ij} n_i n_j$) is

$$\Delta\epsilon_{nn} = \tfrac{16}{3}(1-\nu^2)\frac{b^3}{V}\frac{\sigma_{nn}}{E}. \tag{2.4}$$

Any component of stress acting tangential to the plane of the micro-crack (i.e. $\sigma_{nt} = \sigma_{ij} n_i t_j$, where t_i is parallel to the crack face) gives rise to an increase in the corresponding strain component which is

$$\Delta\epsilon_{nt} = \frac{16}{3}\frac{(1-\nu^2)}{(2-\nu)}\frac{b^3}{V}\frac{\sigma_{nt}}{E}. \tag{2.5}$$

These contributions to the strain are also based on the assumption that interaction between the micro-crack and its neighbours can be ignored.

For the case in which the micro-cracks have random orientation with no preferred alignment, the micro-cracked material will be elastically isotropic on the macro-scale and the strain due to the release of the residual stresses will be a pure dilatation. Suppose there are N micro-cracks per unit volume and let ϵ be the measure of micro-crack density where ϵ is the average of Nb^3 [9]. With $\bar{E}$ and $\bar{\nu}$ denoting the Young's modulus and Poisson's ratio of the micro-cracked material, the total strain following micro-cracking is obtained by averaging the contributions (2.2)–(2.5) over all orientations with the result

$$\epsilon_{ij} = \frac{1+\bar{\nu}}{\bar{E}}\sigma_{ij} - \frac{\bar{\nu}}{\bar{E}}\sigma_{kk}\delta_{ij} + \tfrac{1}{3}\theta^T\delta_{ij} \tag{2.6}$$

where

$$\theta^T = \tfrac{16}{3}(1-\nu^2)\epsilon\frac{\sigma_R}{E}. \tag{2.7}$$

The notation here is deliberately chosen to be the same as that for a dilatational transformation since at the macroscopic level the release of the residual stress is indistinguishable from a transformation. The modulus $\bar{E}$ and Poisson's ratio $\bar{\nu}$ of the micro-cracked material can be obtained from

$$\frac{G}{\bar{G}} = 1 + \frac{32}{45}\frac{(1-\nu)(5-\nu)}{(2-\nu)}\epsilon \tag{2.8}$$

and

$$\frac{B}{\bar{B}} = 1 + \frac{16}{9}\frac{(1-\nu^2)}{(1-2\nu)}\epsilon \tag{2.9}$$

where G and B are the shear and bulk moduli of the uncracked material and $\bar{G}$ and $\bar{B}$ are the corresponding moduli for the micro-cracked material. These estimates of the moduli, which ignore micro-crack interaction, agree with the dilute limit of estimates which approximate interaction [9]. They are reasonably accurate for values of ϵ less than about 0.2 and 0.3, and it is expected that the residual stress contribution in (2.6) will be accurate within this range as well.

2.2. Annular micro-crack ringing a prestressed spherical particle

Now consider a spherical particle which has a residual compressive stress due, for example, to transformation or developed during processing as a result of thermal mismatch between particle and matrix. As depicted in Fig. 3, we suppose that the particle nucleates an axisymmetric micro-crack at its equator with the outer edge of the crack arrested by some feature of the micro-structure. Usually such a micro-crack runs along a grain boundary and arrests at a

boundary junction. We model the situation by taking the particle to be under a residual uniform hydrostatic compression $\sigma_{ij} = -\sigma_R \delta_{ij}$ prior to cracking. If, for example, this residual stress arises as a result of a dilatational transformation strain in the particle of $\epsilon^T_{ij} = \frac{1}{3}\theta^T_p \delta_{ij}$, then

$$\sigma_R = 2E\theta^T_p/[9(1-\nu)]. \tag{2.10}$$

The moduli of the matrix and particle are again taken to be the same. The residual normal traction in the matrix acting across the plane of the potential crack is

$$\sigma = \sigma_0 (b/r)^3 \tag{2.11}$$

where $\sigma_0 = \sigma_R/2$ is the tensile circumferential stress in the matrix just outside the particle, b is the radius of the particle, and r is the distance from the center of the particle.

An annular crack with outer radius a is assumed to form around the equator of the particle as shown in Fig. 3. The volume opening of the crack due to the partial release of the residual stress (2.11) is given approximately by

$$\Delta v = \pi^2(1-\nu^2)ab^2(1-b/a)^2\sigma_0/E \tag{2.12}$$

This formula agrees with accurate numerical results for this problem to within 1 or 2% over the entire range of b/a [10].

Once the micro-crack is nucleated it gives rise to an additional strain contribution (in a material element of volume V) in the direction normal to the crack plane

$$\Delta\epsilon_{nn} = \pi^2(1-\nu^2)\frac{bc^2}{V}\left(1+\frac{2}{3}\frac{c}{b}\right)F\left(\frac{c}{b}\right)\frac{\sigma_{nn}}{E} \tag{2.13}$$

where σ_{nn} is again the macroscopic stress component normal to the plane of the crack and $c = a - b$. The function $F(c/b)$ is 1 when $c/b = 0$ and monotonically decreases to 0.81 when $c/b \to \infty$; it is very close to 1 for $c/b \leqslant 1$. (The formula (2.13) can be derived from results given in [11]. The counterpart to (2.13) for the shear strain contribution $\Delta\epsilon_{nt}$ is not available).

With N noninteracting annular, randomly orientated micro-cracks per unit volume, the strain is still given in terms of the macroscopic stress by (2.6) where now from (2.12)

$$\theta^T = \text{average} \times [N\pi^2(1-\nu^2)ab^2(1-b/a)^2\sigma_0/E]. \tag{2.14}$$

The result (2.13) is not sufficient to determine estimates for $\bar{E}$ and $\bar{\nu}$ since $\Delta\epsilon_{nt}$ is also needed. However, if one assumes that the ratio of $\Delta\epsilon_{nt}/\sigma_{nt}$ to $\Delta\epsilon_{nn}/\sigma_{nn}$ is the same, or at least approximately the same, for the annular crack as for the penny-shaped crack, then $\bar{E}$ and $\bar{\nu}$ can still be obtained from (2.8) and (2.9). Now, however, by comparing (2.4) and (2.13), one sees that the crack density parameter must be taken as

$$\epsilon = \text{average}\left[\frac{3\pi^2 Nbc^2}{16}\left(1+\frac{2}{3}\frac{c}{b}\right)F\left(\frac{c}{b}\right)\right]. \tag{2.15}$$

This formula provides the density of annular micro-cracks measured in an equivalent density of penny-shaped cracks for the purpose of determining the reduction in moduli. The parameter proposed in [9] for arbitrarily shaped micro-cracks, $\epsilon = 2NA^2/(\pi P)$ where A and P are the area and perimeter (inner plus outer) of the crack, provides an excellent simple approximation to (2.15).

3. K_{tip}/K FOR ARBITRARILY SHAPED REGIONS CONTAINING A DILUTE DISTRIBUTION OF RANDOMLY ORIENTATED MICRO-CRACKS

3.1. Uniformly distributed micro-cracks

Some general results for the problem depicted in Fig. 2 will now be presented. The derivation of these results is given in the Appendix. Plane strain deformation of the planar region of Fig. 2 is considered. A semi-infinite crack lies on the negative x_1 axis. Within the region $r \leqslant R(\theta)$, the micro-crack region A_c, the material is governed by (2.6) where θ^T can be thought of as a stress-free dilatational transformation. Within A_c, $\bar{E}$, $\bar{\nu}$ and θ^T are taken to be uniform. Outside this region the material is governed by

$$\epsilon_{ij} = \frac{1+\nu}{E}\sigma_{ij} - \frac{\nu}{E}\sigma_{kk}\delta_{ij} \tag{3.1}$$

The region A_c is restricted to be symmetric with respect to the x_1 axis. The remote, or applied, stress field is specified to be

$$\sigma_{ij} \to \frac{K}{\sqrt{2\pi r}}\tilde{\sigma}_{ij}(\theta), \quad r \to \infty \tag{3.2}$$

where $\tilde{\sigma}_{ij}(\theta)$ are the universal functions characterizing the mode I, plane strain crack-tip fields. We seek the stress intensity factor governing the near-tip fields within the micro-crack region, i.e. we seek K_{tip} where

$$\sigma_{ij} \to \frac{K_{tip}}{\sqrt{2\pi r}}\tilde{\sigma}_{ij}(\theta), \quad r \to 0. \tag{3.3}$$

When $\bar{E} = E$ and $\bar{\nu} = \nu$, K_{tip} is given by [12]

$$K_{tip} = K + \frac{1}{3}\left(\frac{2}{\pi}\right)^{1/2}\frac{E\theta^T}{(1-\nu)} \times \int_0^\pi [R(\theta)]^{1/2}\cos\tfrac{3}{2}\theta\, d\theta \tag{3.4}$$

When $\bar{E}$ and $\bar{\nu}$ differ from E and ν, numerical work is generally required to obtain the relation K_{tip} and K. However, this relation can be obtained in closed form to lowest order in the differences between the moduli governing behavior within and without A_c. Moreover, to lowest order in these differences the contributions to K_{tip} from θ^T and from the reduction in moduli within A_c can be superimposed. We proceed by now considering the case when $\theta^T = 0$.

When $\theta^T = 0$ one can conclude from dimensional analysis alone that

$$K_{tip}/K = F(\bar{E}/E, \nu, \bar{\nu}) \tag{3.5}$$

where F also depends on the shape of A_c but not on its size. However, it can be shown [13] that this relationship can be reduced to a dependence on just two special combinations of the moduli. For present purposes the most convenient choice of moduli parameters is

$$\delta_1 = \frac{1}{1-\nu}\left[\frac{G}{\bar{G}} - 1\right] \tag{3.6}$$

and

$$\delta_2 = \frac{1}{1-\nu}\left[\bar{\nu}\frac{G}{\bar{G}} - \nu\right] \tag{3.7}$$

which both vanish in the absence of any discontinuity across the boundary of A_c. These parameters emerge naturally in the analysis given in the Appendix. With this choice

$$K_{tip}/K = f(\delta_1, \delta_2, \text{shape of } A_c). \tag{3.8}$$

The following result is exact to lowest order in δ_1 and δ_2

$$\frac{K_{tip}}{K} = 1 + (k_1 - \tfrac{5}{8})\delta_1 + (k_2 + \tfrac{3}{4})\delta_2 \tag{3.9}$$

where

$$k_1 = \frac{1}{32\pi}\int_0^\pi (11\cos\theta + 8\cos 2\theta - 3\cos 3\theta) \times \ln[R(\theta)]\,d\theta \tag{3.10}$$

$$k_2 = -\frac{1}{2\pi}\int_0^\pi (\cos\theta + \cos 2\theta)\ln[R(\theta)]\,d\theta. \tag{3.11}$$

Since the collection of terms in each integrand multiplying $\ln[R(\theta)]$ integrates to zero, k_1 and k_2 are unchanged when $R(\theta)$ is replaced by $\lambda R(\theta)$ and are thus dependent on the shape, but not on the size, of A_c. When A_c is a circular region centered at the tip, $k_1 = k_2 = 0$. The circular region has a special role in the development of (3.9), and it is discussed at some length in the Appendix. Numerical results for arbitrarily large moduli differences have been obtained earlier for the problem with a circular region [14]. Some selected results will be compared with (3.9) in the Appendix to give some sense of the range of validity of the lowest order equation.

The above result for K_{tip}/K enables one to determine the jump in the J-integral from integration contours which are entirely within or without A_c. For all contours which circle the crack tip lying outside A_c

$$J = (1-\nu^2)K^2/E \tag{3.12}$$

while for all such contours lying inside A_c

$$J_{tip} = (1-\bar{\nu}^2)K_{tip}^2/\bar{E}. \tag{3.13}$$

Using the relation

$$\frac{(1-\bar{\nu}^2)}{(1-\nu^2)}\frac{E}{\bar{E}} = 1 + \delta_1 - \delta_2 \tag{3.14}$$

one finds to lowest order in δ_1 and δ_2

$$\frac{J_{tip}}{J} = 1 + (2k_1 - \tfrac{1}{4})\delta_1 + (2k_2 + \tfrac{1}{2})\delta_2 \tag{3.15}$$

For exceptional shapes J_{tip} may equal J, but for most shapes it will not.

Combining the contributions from (3.4) for the release in residual stress with those from (3.9) for the reduction in moduli, one finds to lowest order in δ_1 and δ_2

$$\frac{K_{tip}}{K} = 1 + (k_1 - \tfrac{5}{8})\delta_1 + (k_2 + \tfrac{3}{4})\delta_2 + \frac{1}{3}\left(\frac{2}{\pi}\right)^{1/2} \times \frac{E\theta^T}{(1-\nu)K}\int_0^\pi (R(\theta))^{1/2}\cos\tfrac{3}{2}\theta\,d\theta. \tag{3.16}$$

3.2. Nonuniformly distributed micro-cracks

The theory developed in the Appendix permits one to derive expressions for K_{tip}/K for arbitrary distributions of randomly orientated micro-cracks, assuming again that only the lowest order differences in the moduli need be considered. One class of nonuniform distributions leads to particularly simple conclusions and is physically relevant, as will be seen in the next section.

First take $\theta^T = 0$ and consider the effect of shielding due to nonuniform, reduced isotropic moduli within A_c. Suppose, as indicated in Fig. 4, that E and ν govern behavior outside A_c, as before, and that uniform values $\bar{E}_s$ and $\bar{\nu}_s$ hold for $r \leqslant R_s(\theta)$. Moreover, suppose $R_s(\theta) = \lambda R(\theta)$ so that the inner uniform region has the same shape as A_c itself. In the transition region, $R_s(\theta) \leqslant r \leqslant R(\theta)$, we take the moduli to vary continuously from $(\bar{E}_s, \bar{\nu}_s)$ to (E, ν) by "scaling" the moduli differences such that on each radial line from the tip

$$(\delta_1, \delta_2) = (\delta_1^s, \delta_2^s) f(r/R(\theta)) \tag{3.17}$$

where δ_1^s and δ_2^s are derived from $\bar{E}_s$ and $\bar{\nu}_s$ via (3.6) and (3.7) and where $f(x)$ is any continuous function of its argument which decreases monotonically from $f = 1$ at $x = \lambda$ to $f = 0$ at $x = 1$. It is shown in the Appendix that (3.9) is still rigorously valid if δ_1 and δ_2 are replaced by δ_1^s and δ_2^s, respectively. In other words, for this particular class of nonuniform moduli variations the result for K_{tip}/K is the same as for the case where $\bar{E}_s$ and $\bar{\nu}_s$ hold uniformly throughout A_c. To lowest order in δ_1^s and δ_2^s, the result is independent of the details of the transition or of the relative size of the inner uniform region compared to A_c. A numerical example which illustrates this independence was given in [14] for the analogous mode III

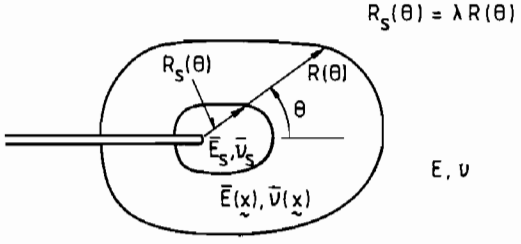

Fig. 4. Geometry of zone with nonuniform micro-cracking.

problem where A_c is a circular region. The numerical example was not limited to lowest order differences and showed that the independence found above held to good approximation even when the moduli differences were quite large.

The contribution to K_{tip} due to release of residual stresses can also be obtained from the result of [12] when θ^T is not uniform. Instead of the second term in (3.4), this contribution is

$$\Delta K_{tip} = \frac{1}{3\sqrt{2\pi}} \frac{E}{(1-\nu)} \int \theta^T \cos\tfrac{3}{2}\theta r^{-3/2}\, dA \quad (3.18)$$

where the integral extends over the upper half of A_c. This contribution does depend on the details of the distribution of θ^T.

4. K_{tip}/K FOR TWO NUCLEATION CRITERIA FOR STATIONARY AND STEADILY GROWING CRACKS

The results of the previous section are now specialized to specific zone shapes dictated by two possible micro-crack nucleation criteria. The first is based on the mean stress; the second is based on the maximum normal stress. In each case in this section it will be assumed that there is no preferred orientation to the micro-cracks so that the reduced moduli are isotropic. Results for both stationary cracks and cracks which have achieved steady-state growth conditions will be given so as to assess the potential for crack growth resistance following initiation. In every example in this paper the zone shape and size are determined using the unperturbed elastic stress field (3.2) since this is consistent with our limited aim of obtaining just the lowest order contributions to K_{tip}. The perturbation of the size of the zone is likely to be relatively unimportant for the effect of the reduced moduli even for non-dilute crack distributions since the lowest order results for K_{tip}/K are independent of zone size, as discussed in the previous section. The effect of the perturbation on the contribution of the release in residual stress is essentially the same as in the pure transformation problem which was treated in [12].

4.1. Stationary crack with nucleation at a critical mean stress

With $\sigma_m = \frac{1}{3}\sigma_{kk}$ as the mean stress, suppose micro-cracks begin nucleating at σ_m^c and the nucleation is complete at σ_m^s with a variation in micro-crack density N as indicated in Fig. 5(a). To lowest order, the elastic stress distribution (3.2) can be used to determine the zone shape and the distribution of the micro-crack density within the zone. The distribution of the density and the relation of the inner region of uniform moduli to the full micro-crack region fits precisely into the situation discussed in Section 3.2 and sketched in Fig. 4. Thus, the change in K_{tip} due to the moduli reduction is the same, to lowest order, as when the micro-cracks are uniformly distributed throughout the zone. We will therefore restrict attention to the simplified nucleation criterion indicated in Fig. 5(b) and take

$$\text{micro-crack density} = 0 \text{ for } (\sigma_m)_{max} < \sigma_m^c$$
$$= N \text{ for } (\sigma_m)_{max} \geq \sigma_m^c. \quad (4.1)$$

The θ^T-contribution to K_{tip} does depend on the distribution of the micro-crack density, but this can be evaluated fairly simply using (3.18) if desired. Here only the results for the simplified nucleation criterion (4.1) will be given. There will be a transition region just within the boundary to A_c in which the micro-crack density varies from zero to the saturated value, but in the limit corresponding to the lowest order problem the transition region shrinks to zero.

Imposing $\sigma_m = \sigma_m^c$ on the elastic field (3.2), one finds

$$R(\theta) = \frac{2}{9\pi}(1+\nu)^2 \left(\frac{K}{\sigma_m^c}\right)^2 \cos^2\left(\frac{\theta}{2}\right). \quad (4.2)$$

The boundary of the micro-crack zone is shown in Fig. 6(a). Then, evaluating k_1 and k_2 in (3.10) and (3.11), one obtains $k_1 = 3/16$ and $k_2 = -1/4$. The θ^T-contribution to (3.16) is found to be identically zero, and thus (3.16) becomes

$$K_{tip}/K = 1 - (7/16)\delta_1 + (1/2)\delta_2. \quad (4.3)$$

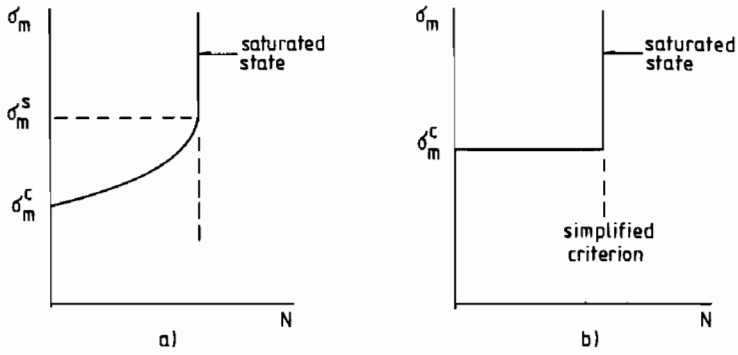

Fig. 5. Variation of micro-crack density N with means stress.

To specialize the result even further we will use the results (2.8) and (2.9) for the reduced moduli $\bar{G}$ and $\bar{B}$ in terms of the crack density parameter ϵ which in turn is given by the average of Nb[3], or by (2.15), or by any other appropriate choice depending on the nature of the micro-cracking. To lowest order in ϵ, one can show that

$$\bar{\nu} = \nu - \frac{16\nu}{15}\frac{(3-\nu)(1-\nu^2)}{(2-\nu)}\epsilon \tag{4.4}$$

and

$$\delta_1 = \frac{32(5-\nu)}{45(2-\nu)}\epsilon, \qquad \delta_2 = \frac{16\nu(1-8\nu+3\nu^2)}{45(2-\nu)}\epsilon$$
$$= 1.99\epsilon\,(\nu=\tfrac{1}{3}), \qquad = -0.095\epsilon\,(\nu=\tfrac{1}{3}) \tag{4.5}$$

and thus

$$\frac{K_{\text{tip}}}{K} = 1 - \frac{2(35-11\nu+32\nu^2-12\nu^3)}{45(2-\nu)}\epsilon$$
$$= 1 - 0.919\epsilon\,(\nu=\tfrac{1}{3}). \tag{4.6}$$

4.2. Steadily growing crack with nucleation at a critical mean stress

A crack which has extended at constant K has a wake of micro-cracks as indicated in Fig. 6(a). With the nucleation criterion (4.1) in effect, the leading edge of the micro-crack zone is given by (4.2) for $|\theta| < 60^\circ$, and the half-height of the zone is given by

$$H = \frac{\sqrt{3}\,(1+\nu)^2}{12\pi}\left(\frac{K}{\sigma_m^c}\right)^2 \tag{4.7}$$

The values of k_1 and k_2, which have been computed by numerical integration, are

$$k_1 = 0.0166 \quad \text{and} \quad k_2 = -0.0433. \tag{4.8}$$

Equation (3.16) gives

$$\frac{K_{\text{tip}}}{K} = 1 - 0.608\delta_1 + 0.707\delta_2$$
$$- \frac{1}{4\pi\sqrt{3}}\frac{(1+\nu)}{(1-\nu)}\frac{E\theta^{\text{T}}}{\sigma_m^c}$$
$$= 1 - 0.608\delta_1 + 0.707\delta_2$$
$$- \frac{E\theta^{\text{T}}}{2(1-\nu)K}\left(\frac{H}{\pi\sqrt{3}}\right)^{1/2} \tag{4.9}$$

where the θ^{T}-contribution is the same as that obtained in [12] and [15] for the corresponding transformation problem. Equation (4.5) for δ_1 and δ_2 still pertain and for $\nu = 1/3$

$$K_{\text{tip}}/K = 1 - 1.278\epsilon - 0.3215\,E\theta^{\text{T}}\sqrt{H}/K. \tag{4.10}$$

By comparing (4.6) and (4.10), one notes that the shielding contribution due to moduli reduction is about 40% larger for the growing crack than for the stationary crack. This will add to crack growth resistance but the major source of resistance is likely to come from the release of residual stress (i.e. from θ^{T}). Even without growth, however, moduli reduction provides some shielding according to (4.6), although how much extra toughness this generates cannot be predicted without knowledge of the toughness of the micro-cracked material within A_c, as already emphasized.

4.3. Stationary crack with nucleation at a critical maximum normal stress

Now suppose that the micro-cracks are still nucleated with no preferred orientations so that within A_c the stress–strain relation is still (2.6), but suppose that nucleation occurs when the maximum principal stress σ_1 reaches a critical tensile value σ_c, i.e.

$$\text{micro-crack density} = 0 \quad (\sigma_1)_{\max} < \sigma_c$$
$$= N \quad (\sigma_1)_{\max} \geqslant \sigma_c \tag{4.11}$$

where, as before, $(\ )_{\max}$ signifies the maximum value attained over the history.

The boundary to A_c as determined by (3.2) is

$$R(\theta) = \frac{1}{2\pi}\left(\cos\frac{\theta}{2} + \frac{1}{2}\sin|\theta|\right)^2 (K/\sigma_c)^2 \tag{4.12}$$

and this is shown in Fig. 6(b). The values of k_1 and k_2 have been obtained by numerical integration of (3.10) and (3.11) with the result

$$k_1 = 0.0779 \quad \text{and} \quad k_2 = -0.0756. \tag{4.13}$$

Equation (3.16) gives

$$\frac{K_{\text{tip}}}{K} = 1 - 0.547\delta_1 + 0.674\delta_2 - E\theta^{\text{T}}/[6\pi(1-\nu)\sigma_c]$$
$$= 1 - 0.547\delta_1 + 0.674\delta_2 - 0.1060\,E\theta^{\text{T}}$$
$$\times \sqrt{H}/[(1-\nu)K] \tag{4.14}$$

where the half-height of A_c from (4.12) is obtained at $\theta = 74.84^\circ$ and is

$$H = 0.2504(K/\sigma_c)^2. \tag{4.15}$$

For $\nu = 1/3$ and with δ_1 and δ_2 given by (4.5), (4.14) specializes to

$$\frac{K_{\text{tip}}}{K} = 1 - 1.153\epsilon - 0.159\,E\theta^{\text{T}}\sqrt{H}/K \tag{4.16}$$

4.4. Steadily growing crack with nucleation at a critical maximum normal stress

Now the zone A_c is specified by (4.12) for $|\theta| \leqslant 74.84^\circ$ and by $|x_2| = H$ for $|\theta| > 74.84^\circ$ where H is given by (4.15). Evaluating the integrals in (3.10), (3.11) and (3.16) numerically, one finds

$$\frac{K_{\text{up}}}{K} = 1 - 0.673\delta_1 + 0.822\delta_2$$
$$- 0.1329\,E\theta^{\text{T}}/[(1-\nu)\sigma_c]$$
$$= 1 - 0.673\delta_1 + 0.822\delta_2$$
$$- 0.2656E\theta^{\text{T}}\sqrt{H}/[(1-\nu)K] \tag{4.17}$$

which for $\nu = 1/3$ and δ_1 and δ_2 given by (4.5) becomes

$$\frac{K_{\text{tip}}}{K} = 1 - 1.417\epsilon - 0.398\,E\theta^{\text{T}}\sqrt{H}/K. \tag{4.18}$$

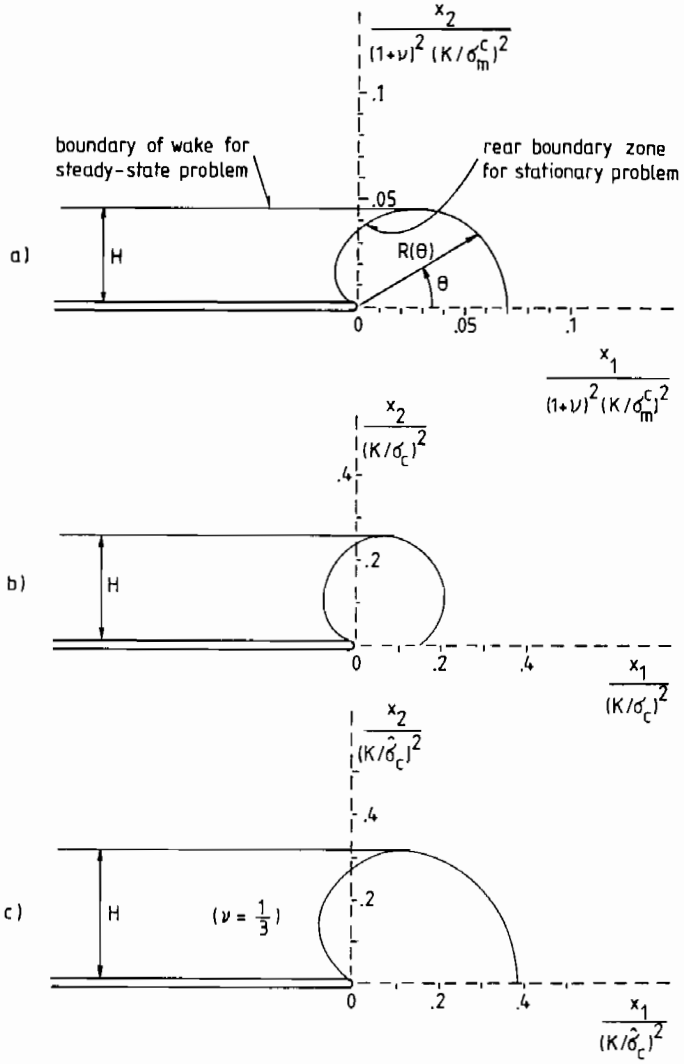

Fig. 6. Zones of micro-cracked material for stationary and steadily growing cracks for three nucleation criteria. (a) Critical mean stress criterion. (b) Critical maximum principal stress criterion. (c) Criterion based on a critical value of $\sqrt{(\sigma_{ij}\sigma_{ij})}$ for $\nu = 1/3$.

The predictions for this case are not very different from those based on a critical mean stress. The shielding due reduction in moduli is larger in each case by about the same amount for the steadily-growing crack compared to the stationary crack. For nucleation at a critical maximum principal stress there is some shielding even for the stationary problems due to θ^T. This is not the case for nucleation at a critical mean stress.

4.5. Effect of zone shape on shielding

For cases, such as those discussed above, in which the moduli of the micro-cracked material are isotropic and the release of residual stress gives a pure dilatation θ^T, the general result (3.16) can be used to gain qualitative insight on the effect of zone shape on shielding.

For the θ^T-contribution, it follows immediately that, because $R(\theta)^{1/2}$ is modulated by $\cos(3\theta/2)$ in (3.16), decreases in R in the range $|\theta| < 60°$ and increases in R in the range $|\theta| > 60°$ will increase shielding.

The trend is similar for shielding due to the reduction in moduli. Note from (4.5) that δ_1 is generally much larger in magnitude than δ_2 and will generally be the predominate of the two parameters in determining K_{tip}. By (3.16), therefore, the influence of shape on K_{tip} comes about mainly through k_1. By (3.10), the integral for k_1 involves $\ln[R(\theta)]$ modulated by

$$f(\theta) = \frac{1}{32\pi}(11\cos\theta + 8\cos 2\theta - 3\cos 3\theta). \quad (4.19)$$

This function is plotted in Fig. 7, and it is seen to be positive for $|\theta| < 70.5°$ and negative for $|\theta| > 70.5°$. Thus, with a circular shape as reference ($k_1 = k_2 = 0$), shape changes involving decreases in R for $|\theta| < 70.5°$ and increases for $|\theta| > 70.5°$ will increase shielding. However, the influence of shape change is not nearly as strong as in the case of the

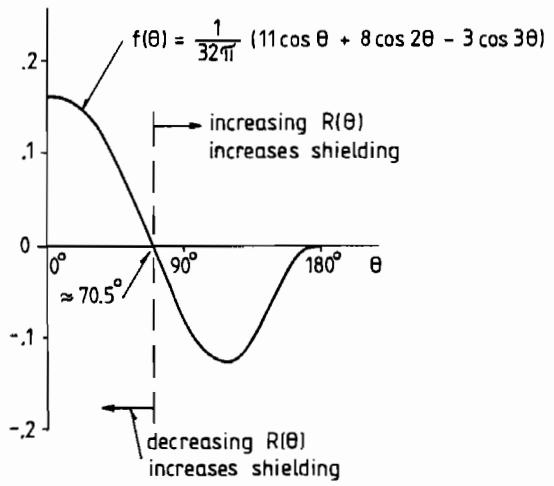

Fig. 7. Plot of the function $f(\theta)$ appearing in the expression for k_1 and its implication for changes in shielding stemming from changes in shape of micro-crack zone.

θ^T-contribution. The examples worked out above suggest that k_1 and k_2 are generally quite small so that shielding will not be markedly different than that afforded by a circular zone centered at the tip. Even the addition of the wake in the steady-state problems only increases the shielding by 30–40% over the circular zone.

5. SOME RELATED RESULTS

5.1. Anisotropic micro-cracking—stationary crack

A material which nucleates micro-cracks with planes which are perpendicular to the maximum principal stress σ_I was considered in [16]. A closed form relation between K_{tip} and K was obtained which is not limited to dilute levels of micro-cracks. In monotonically increasing uniaxial tension the stress-strain relation of the material was assumed to have the form shown in Fig. 1 with

$$\begin{aligned} \epsilon &= \sigma/E && \sigma < \sigma_c \\ &= g(\sigma) && \sigma_c < \sigma < \sigma_s \\ &= \epsilon^T + \sigma/\bar{E}_s && \sigma > \sigma_s \end{aligned} \tag{5.1}$$

where $\bar{E}_s$ is the incremental modulus associated with the saturated micro-crack density and $g(\sigma)$ is a monotone function which characterizes the transition from uncracked to fully saturated conditions. The uniaxial "transformation" strain ϵ^T resulting from release of residual stress by the micro-cracks was not considered in [16] but can be included without any alteration of the analysis. For monotonic proportional stressing histories, the assumption that the micro-cracks form normal to the direction of the maximum principal stress leads to a relation between σ_1 and the maximum principal strain, ϵ_1, which is the same as (5.1). The other two principal strain components are taken to be unaffected by the micro-cracking, i.e.

$$\begin{aligned} E\epsilon_{II} &= \sigma_{II} - \nu(\sigma_I + \sigma_{III}) \\ E\epsilon_{III} &= \sigma_{III} - \nu(\sigma_I + \sigma_{II}). \end{aligned} \tag{5.2}$$

The result of [16] is limited to a stationary macro-crack. For then, one can reasonably expect the stress history at every material point will be monotonically proportional (at least to a good approximation) if K is increased monotonically. It was noted in [16] that a deformation theory (i.e. a small strain, nonlinear elasticity theory) exists which coincides with stress–strain behavior of the material described above when the stressing is proportional. Thus it was argued that for this material with a stationary crack the J-integral is path-independent so that

$$J_{tip} = J. \tag{5.3}$$

This, in turn, led to the relation

$$\frac{K_{tip}}{K} = \left[1 + \frac{\beta}{(1-\nu^2)}\left(\frac{E}{\bar{E}_s} - 1\right)\right]^{-1/2} \tag{5.4}$$

where $\beta = 1.0942$. The "transformation" strain ϵ^T resulting from release of residual stress does not affect the relation for the stationary crack. The relation is also independent of both σ_c and σ_s as well as $g(\sigma)$.

To draw comparisons with results in the previous section, suppose that the micro-cracks nucleated are penny-shaped with a density N per unit volume in the saturated state. Since the planes of the micro-cracks all lie perpendicular to the maximum principal stress, if follows from (2.4) that

$$\frac{E}{\bar{E}_s} = 1 + \tfrac{16}{3}(1-\nu^2)\epsilon \tag{5.5}$$

where ϵ is the average of Nb^3. [Equivalently, (5.5) holds for annular micro-cracks if ϵ is given by (2.15).] Of course, (5.5) ignores the interaction among micro-cracks. Combining (5.4) and (5.5), one finds

$$\frac{K_{tip}}{K} = [1 + 5.836\epsilon]^{-1/2} = 1 - 2.918\epsilon + \cdots \tag{5.6}$$

Noting the corresponding lowest order estimates in (4.6) and (4.16) for isotropically orientated micro-cracks, one concludes that micro-cracks nucleated perpendicular to the maximum principal stress result in more effective shielding at the same level of micro-crack density.

5.2. Anisotropic micro-cracking—steadily growing crack

Results as general as those for the stationary crack just quoted cannot be generated in the same way for the steady-state crack growth problem since the path-independence of the J-integral can no longer be invoked. Complete lowest order results such as those derived in Section 4 for the isotropic case could be obtained but are not yet available. However, lowest order results are available for the contribution to K_{tip} due to release of residual stress.

In the simplest case, suppose that all micro-cracks nucleate with planes normal to the maximum principal stress when

$$(\sigma_1)_{\max} = \sigma_c \tag{5.7}$$

so that the "inelastic" strain resulting from the release of the residual stress is

$$\epsilon_{ij}^T \simeq \epsilon^T n_i n_j \tag{5.8}$$

where $\mathbf{n}$ is the unit vector in the direction of the maximum principal stress. The lowest order approximation to the micro-crack zone is that shown in Fig. 6(b) for the steadily growing crack. The micro-cracks are nucleated along the leading boundary of the micro-crack zone and this establishes the variation of the orientation of the micro-cracks throughout the zone. The variation is independent of x_1 to lowest order.

The problem characterized by (5.7) and (5.8) is exactly equivalent to the uniaxial transformation problem analysed in [17]. The result (which has been rederived analytically by the present author) is

$$\frac{K_{tip}}{K} = 1 - 0.2504\frac{E\epsilon^T}{(1-\nu^2)\sigma_c}$$

$$= 1 - 0.5004\frac{E\epsilon^T\sqrt{H}}{K(1-\nu^2)} \tag{5.9}$$

where H is given by (4.15). An expression for ϵ^T in terms of the residual stress and the micro-crack density may be obtained immediately using either (2.2) or (2.12).

5.3. Isotropic micro-cracking with a special nucleation condition

A special small strain, nonlinear elastic constitutive law (a hyperelastic law) was introduced in [18] to model micro-cracking and, at the same time, to preserve the path-independence of the J-integral when stressing is monotonically proportional. Thus, as in the example discussed above, it is possible to link the near-tip K to the remote K for the *stationary crack problem* using just the path-independence of J. In this instance, however, the moduli of the material with saturated micro-cracking are isotropic so that

$$\frac{1-\bar{\nu}^2}{\bar{E}}K_{tip}^2 = \frac{1-\nu^2}{E}K^2 \tag{5.10}$$

where $\bar{\nu}$ and $\bar{E}$ are the Poisson's ratio and Young's modulus of the material in the saturated state.

The constitutive law proposed in [18] is

$$E\epsilon_{ij} = (h(\hat{\sigma}) + \nu)\sigma_{ij} - \nu\sigma_{kk}\delta_{ij} \tag{5.11}$$

where $\hat{\sigma} = (\sigma_{ij}\sigma_{ij})^{1/2}$ and

$$h(\hat{\sigma}) = [1 - \tfrac{16}{9}\epsilon(\hat{\sigma})]^{-1}. \tag{5.12}$$

The micro-crack density parameter ϵ is the same as that used here. It is regarded as a function of $\hat{\sigma}$ and is taken to be zero for $\hat{\sigma} < \hat{\sigma}_c$ and to increase continuously until it attains the saturation value ϵ_s when $\hat{\sigma} = \hat{\sigma}_s$. The claim in [18] is that the moduli in (5.11) for a given value of ϵ are a good approximation to the moduli derived from self-consistent theory in [9].

With $h_s = [1 - 16\epsilon_s/9]^{-1}$, the values of $\bar{\nu}$ and $\bar{E}$ for the material at saturation from (5.11) are

$$\bar{E} = h_s^{-1}E \quad \text{and} \quad \bar{\nu} = h_s^{-1}\nu. \tag{5.13}$$

Thus, (5.10) gives

$$\frac{K_{tip}}{K} = \left[\frac{(1-\nu^2)h_s}{h_s^2 - \nu^2}\right]^{1/2} \tag{5.14}$$

which is plotted as a function of ϵ_s in Fig. 8 for $\nu = \frac{1}{3}$.

We have applied the theory of Section 3 to this special constitutive law for the limiting case where $\hat{\sigma}_c = \hat{\sigma}_s$ so that the material develops the saturated level of micro-cracking ϵ_s as soon as $\hat{\sigma} = (\sigma_{ij}\sigma_{ij})^{1/2}$ attains $\hat{\sigma}_c$. The moduli within A_c are uniform to lowest order in ϵ_s and are given by (5.13). Then, by

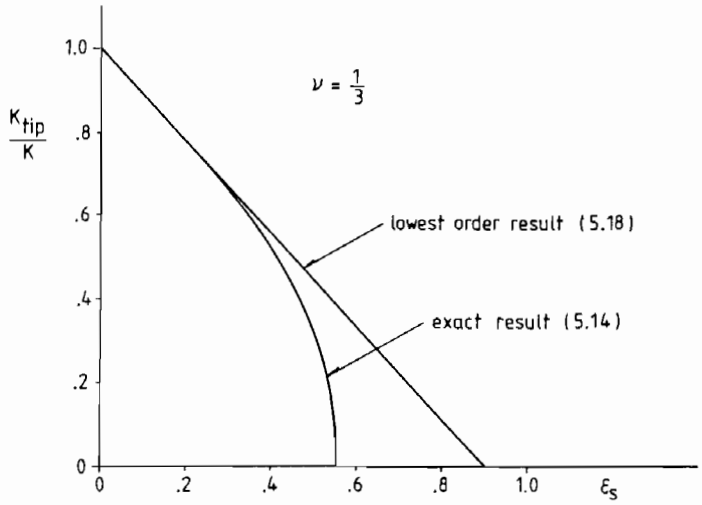

Fig. 8. Comparison of exact and lowest order results for stationary crack in special material.

Table 1. $(K_{tip}/K) - 1$ for $\nu = 1/3$ from lowest order theory expressed in terms of crack density parameter ϵ measuring equivalent density of penny-shaped cracks. Equation numbers from the paper are given in brackets

Nucleation criterion	Critical mean stress $\sigma_m = \sigma_m^c$	Critical maximum principal stress $\sigma_1 = \sigma_c$	Critical maximum principal stress $\sigma_1 = \sigma_c$	Critical $\hat{\sigma} = \sqrt{\sigma_{ij}\sigma_{ij}}$ $\hat{\sigma} = \hat{\sigma}_c$
Orientation distribution of micro-cracks	Isotropic	Isotropic	Anisotropic (micro-cracks normal to maximum principal stress)	Isotropic
Stationary crack	-0.92ϵ (4.6)	-1.15ϵ $-0.16\, E\theta^T\sqrt{H}/K$ (4.16)	-2.92ϵ (5.6)	-1.11ϵ $-0.063\, E\theta^T\sqrt{H}/K$ (5.18)
Steady-state crack	-1.28ϵ $-0.32\, E\theta^T\sqrt{H}/K$ (4.10)	-1.42ϵ $-0.39\, E\theta^T\sqrt{H}/K$ (4.18)	[a] $-0.56\, E\epsilon^T\sqrt{H}/K$ (5.9)	-1.42ϵ $-0.35\, E\theta^T\sqrt{H}/K$ (5.20)

[a] ϵ-Contribution not available.

(3.6) and (3.7)

$$\delta_1 = \frac{16}{9(1-\nu^2)}\epsilon_s, \quad \delta_2 = \frac{-16\nu^2}{9(1-\nu^2)}\epsilon_s$$
$$= 2\epsilon_s(\nu = \tfrac{1}{3}), \quad = -\tfrac{2}{9}\epsilon_s(\nu = \tfrac{1}{3}) \quad (5.15)$$

to lowest order in ϵ_s. [Note that these expressions do not agree exactly with those in (4.5) since the constitutive relation (5.11) is not exact in the dilute limit. Nevertheless, the numerical agreement for δ_1, in particular, is extremely good for $\nu = 1/3$ and is exact for $\nu = 0$.]

The boundary of A_c for the stationary crack is specified by [see Fig. 6(c)]

$$R(\theta) = \frac{1}{\pi}\left(\frac{K}{\hat{\sigma}_c}\right)^2 \times \left[(1+2\nu^2)\cos^2\frac{\theta}{2} + \frac{1}{4}\sin^2\theta\right]. \quad (5.16)$$

One can show by direct, but nontrivial, integration that

$$2k_1\delta_1 + 2k_2\delta_2 = \tfrac{1}{4}\delta_1 - \tfrac{1}{2}\delta_2 \quad (5.17)$$

so that, by (3.15), the relation $J_{tip} = J$ is indeed verified. Thus, to lowest order in ϵ_s, the present theory coincides with (5.14). For $\nu = 1/3$, we find

$$K_{tip}/K = 1 - (10/9)\epsilon_s - 0.0352\, E\theta^T/\hat{\sigma}_c \quad (5.18)$$

where the contribution due to θ^T, which is not included in (5.11), has also been computed. The lowest order prediction (excluding the θ^T-contribution) is also shown in Fig. 8 and it is seen that it supplies a good approximation for values of ϵ_s up to about 0.4 corresponding to about a 50% reduction in K_{tip}.

Application of the theory to the *steadily growing crack* is straight-forward. The micro-crack zone A_c is shown in Fig. 6(c), and the half-height of the zone for $\nu = 1/3$ is

$$H = 0.311(K/\hat{\sigma}_c)^2. \quad (5.19)$$

Using numerical integration to evaluate the integrals in (3.11) and (3.16), one finds to lowest order in ϵ_s for $\nu = 1/3$

$$\frac{K_{tip}}{K} = 1 - 1.42\epsilon_s - 0.194\, E\theta^T/\hat{\sigma}_c$$
$$= 1 - 1.42\epsilon_s - 0.348\, E\theta^T\sqrt{H}/K. \quad (5.20)$$

Here, a θ^T-contribution due to release of residual stress has again been included, where θ^T has also been taken to be uniform within A_c consistent with assumption made about the micro-crack nucleation.

The shielding effects implied by this material model are very similar to those found for the other two models in Section 4.

6. CONCLUSIONS

All the lowest order results for the various models for $\nu = 1/3$ have been assembled in Table 1 expressed in terms of the crack density parameter ϵ which measures the equivalent density of penny-shaped cracks. The three models which assume isotropically distributed micro-cracks all give very similar results. In each of the three cases, the increase in shielding of the growing crack over the stationary crack due to the reduction in moduli (the ϵ-contribution) is between 30 and 40%. Values of ϵ of about 0.3 near the crack tip have been observed [3], corresponding to about a 40% reduction in K_{tip} due to this effect. The shielding contribution due to release in residual stress (the θ^T-contribution) is exactly the same as in the corresponding transformation problem, and the shielding is significantly greater for the steadily growing crack than for the stationary crack. It would appear that strong resistance curve behavior would stem mainly from the release of the residual stresses.

The results for the anisotropic case, where the micro-cracks are nucleated perpendicular to the maximum principal stress direction, are larger, by a factor of about two, compared to the isotropic cases at the same micro-crack density. If micro-cracks are nucleated with a high degree of alignment, the saturated density would likely be less than in the isotropic case because of fewer available nucleation sites. A

direct comparison of the two cases may not be meaningful therefore.

The results of Table 1 probably bracket what would be expected from any reasonable continuum model. More observational data such as that in [3] is needed before it will be possible to settle on any one model. At issue are both the stress dependence of nucleation and the orientation distribution of the micro-cracks. In addition, a deeper understanding is needed of the saturated micro-cracked state and its relation to the inherent fracture toughness of the micro-cracked material.

Finally, it should be re-emphasized that the present results, for the most part, have been limited to lowest order accuracy. Numerical calculations such as those in [18] will be needed to obtain accurate estimates of shielding when K_{tip}/K is less than about $\frac{1}{2}$. Approximate ways to extend the range of accuracy of the lowest order formulas suggest themselves. For example, without altering the lowest order accuracy, one may modify the basic result (3.9) to

$$\frac{K_{tip}}{K} = [1 - (k_1 - \tfrac{5}{8})\delta_1 - (k_2 + \tfrac{3}{4})\delta_2]^{-1}. \qquad (6.1)$$

For each example considered here, this change ensures that $K_{tip}/K \to 0$ as δ_1 and δ_2 become unbounded, as should be the case. The improvement in the range of accuracy can be quite dramatic as is illustrated by the example for a circular region ($k_1 = k_2 = 0$) in Fig. 12 shown later in the Appendix. It is recommended that the modified lowest order result (6.1) be used when δ_1 and δ_2 are not very small.

Acknowledgement—This work was supported in part by grants DMR-83-16979 and MSM-84-16392 and in part by the Division of Applied Sciences, Harvard University. The writer is indebted to A. G. Evans for stimulating the work and to M. Rühle for discussions of his experimental observations.

REFERENCES

1. H. Hübner and W. Jillek, *J. Mater. Sci.* **12,** 117 (1977).
2. R. Knehans and R. Steinbrech, *J. Mater. Sci. Lett.* **1,** 327 (1982).
3. M. Rühle, A. G. Evans, R. M. McMeeking, P. G. Charalambides and J. W. Hutchinson. To be published.
4. R. G., Hoagland and J. D. Embury, *J. Am. Ceram. Soc.* **63,** 404 (1980).
5. D. R. Clarke, *Comm. Am. Ceram. Soc.* C-15, January (1984).
6. K. T. Faber and A. G. Evans, *Acta metall.* **31,** 577 (1983).
7. Y. Fu and A. G. Evans, *Acta metall.* **33,** 1515 (1985).
8. A. G. Evans and Y. Fu, *Acta metall.* **33,** 1525 (1985).
9. B. Budiansky and R. J. O'Connell, *Int. J. Solids Struct.* **12,** 81 (1975).
10. D. Shum and J. W. Hutchinson, work in progress on various micro-crack configurations.
11. H. Tada, P. C. Paris and G. R. Irwin, *Handbook for Stress Analysis of Cracks*, 2nd edn. Del Research (1985).
12. B. Budiansky, J. W. Hutchinson and J. C. Lambropoulos, *Int. J. Solids Struct.* **19,** 337 (1983).
13. J. Dundurs, *J. appl. Mech.* **36,** 650 (1969).
14. P. S. Steif, *J. appl. Mech.* To be published.
15. R. M. McMeeking and A. G. Evans, *J. Am. Ceram. Soc.* **65,** 242 (1982).
16. M. Ortiz, *J. appl. Mech.* To be published.
17. J. C. Lambropoulos, *Int. J. Solids Struct.* **22,** 1083 (1986).
18. P. Charalambides and R. M. McMeeking. To be published.
19. J. W. Hutchinson, Harvard University, Report DEAP S-8 (1974).
20. J. R. Rice, *Int. J. Solids Struct.* **21,** 781 (1985).

APPENDIX: K_{tip} ANALYSIS

The Appendix is divided into three main sections. The first gives a basic solution for the stress intensity at a crack tip induced by an arbitrary distribution of transformation strain (i.e. plastic strain) in its vicinity. The general result (3.9) for arbitrarily shaped regions is constructed using two auxiliary solutions. One of these auxiliary solutions can be written down immediately using the basic solution of the first section. The other which pertains to a circular region is then derived and is related to numerical results for arbitrarily large moduli differences in the third section. A short final section deals with zones containing nonuniform micro-crack distributions.

K_{tip} *for Arbitrary Distributions of Transformation Strain*

A solution was derived in [19] for the stresses and the stress intensity factor at a semi-infinite crack induced by two symmetrically placed "spots" of area dA which have undergone an in-plane transformation strain, as indicated in Fig. 9. We consider plane strain, mode I behavior so that if the transformation strain in the upper spot is $(\epsilon^T_{11}, \epsilon^T_{22}, \epsilon^T_{12})$ then the corresponding strain in the lower spot is $(\epsilon^T_{11}, \epsilon^T_{22}, -\epsilon^T_{12})$. Here we present only the result for the stress intensity factor induced by the transformation in the differential spots:

$$dK_{tip} = (8\pi)^{-1/2}(1-\nu^2)^{-1} E\, dA\, r^{-3/2} h_{\alpha\beta}(\theta)\epsilon^T_{\alpha\beta} \qquad (A1)$$

where (r, θ) are planar-polar coordinates to the upper spot and

$$h_{11} = \tfrac{1}{4}(\cos\tfrac{3}{2}\theta + 3\cos\tfrac{7}{2}\theta)$$
$$h_{22} = \tfrac{1}{4}(7\cos\tfrac{3}{2}\theta - 3\cos\tfrac{7}{2}\theta)$$
$$h_{12} = h_{21} = \frac{3}{4}\left(\sin\frac{7\theta}{2} - \sin\frac{3\theta}{2}\right). \qquad (A2)$$

The stress intensity induced by a symmetric distribution of transformation strain is given by the superposition of (A1) as long as

$$\lim_{r\to 0} r^{-1/2}\epsilon^T_{\alpha\beta} = 0. \qquad (A3)$$

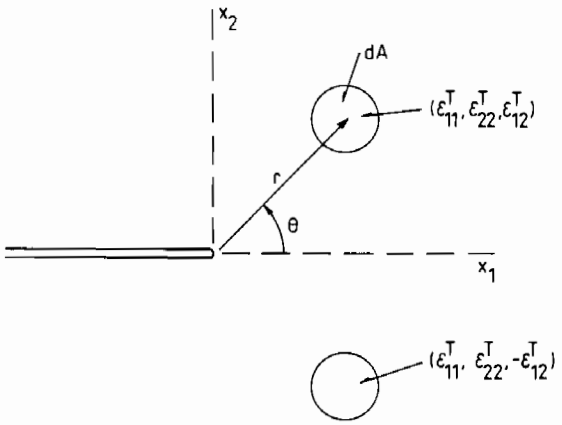

Fig. 9. Geometry associated with equation (A1).

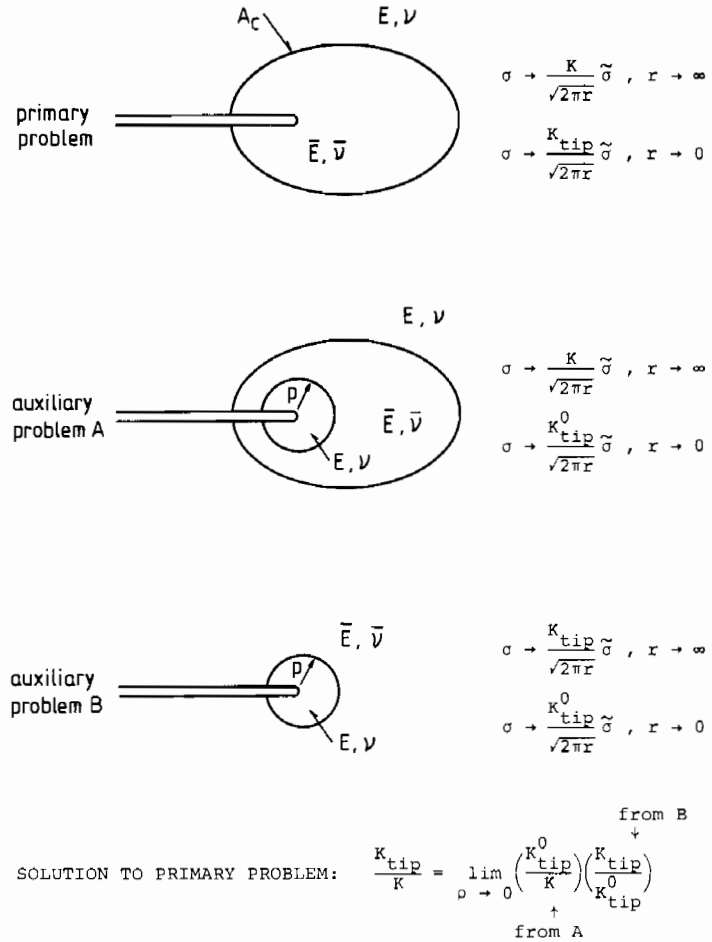

Fig. 10. Definitions of auxiliary problems *A* and *B* and their use in construction of the solution to the primary problem.

Thus, assuming (A3) holds

$$K_{tip} = (8\pi)^{-1/2}\frac{E}{(1-\nu^2)}\int r^{-3/2}h_{\alpha\beta}(\theta)\epsilon^{T}_{\alpha\beta}\,dA \qquad (A4)$$

plus any contribution due to remote applied stresses. The area integral in (A4) is taken over the transformed region in the upper-half plane. This result is the same as that used in [17]; related developments are discussed in [20].

The expressions given in the body of this paper for the contributions to K_{tip} due to release of residual stress have been derived from (A4). Their derivation is similar to one given in [12] so we will not dwell further with this aspect. We turn to the more difficult part of the derivation concerning the change in K_{tip} due to the reduction in moduli within a region A_c surrounding the tip.

K_{tip} *Due to Reduced Moduli Within* A_c

Our objective is the determination of K_{tip}/K when the symmetric region A_c surrounding the semi-infinite crack tip has different, but uniform, moduli $(\bar{E}, \bar{\nu})$ from the moduli (E, ν) outside A_c. Plane strain conditions are assumed and only lowest order accuracy is sought, i.e. we seek the result for K_{tip}/K which is linearized in the moduli differences δ_1 and δ_2 defined in (3.6) and (3.7). The solution is constructed using solutions to two auxiliary problems denoted by "A" and "B" in Fig. 10. The construction indicated in Fig. 10 is actually valid for arbitrary large moduli differences, assuming the two auxiliary solutions were known for arbitrarily large differences. The reason for dividing the problem into two in the manner shown will be clearer in the exposition which follows. Curiously, the lowest order solution to problem A can be written down almost immediately using (A4). The lowest order solution to problem B is also simply obtained although a back-handed procedure has been employed in the process. Once the solutions to the two auxiliary problems are in hand, the ratio of the stress intensity factors sought is given by

$$\frac{K_{tip}}{K} = \left(\frac{K^0_{tip}}{K}\right)\left(\frac{K_{tip}}{K^0_{tip}}\right) \qquad (A5)$$

where K^0_{tip}/K is the ratio of the near-tip to remote intensity factor in problem A and K^0_{tip}/K_{tip} is the corresponding ratio in problem B.

To generate the solution to *auxiliary problem A*, let $\mathbf{M}$ denote the compliances of the isotropic material outside A_c and inside the circular region, $r \leqslant \rho$. Let $\bar{\mathbf{M}}$ be the compliances of the isotropic material inside A_c, but excluding the inner circular region, so that within this intermediate region

$$\begin{aligned}\epsilon_{\alpha\beta} &= \bar{M}_{\alpha\beta\kappa\gamma}\sigma_{\kappa\gamma} \\ &= M_{\alpha\beta\kappa\gamma}\sigma_{\kappa\gamma} + (\bar{M}_{\alpha\beta\kappa\gamma} - M_{\alpha\beta\kappa\gamma})\sigma_{\kappa\gamma}.\end{aligned} \qquad (A6)$$

With the identification

$$\epsilon^{T}_{\alpha\beta} = (\bar{M}_{\alpha\beta\kappa\gamma} - M_{\alpha\beta\kappa\gamma})\sigma_{\kappa\gamma} \qquad (A7)$$

one can use (A4) to write

$$K^0_{tip} = K + (8\pi)^{-1/2}\frac{E}{(1-\nu^2)}\int r^{-3/2}h_{\alpha\beta}(\theta)\epsilon^{T}_{\alpha\beta}\,dA \qquad (A8)$$

where the area integral extends over the upper half of A_c, excluding the inner circular region. Of course, for arbitrarily large differences in $\bar{\mathbf{M}}$ and $\mathbf{M}$ the stress, and therefore also $\epsilon^T_{\alpha\beta}$, is not known a priori. However, to lowest order in the compliance differences, the stress in (A7) is the remote stress field (3.2), which is the limiting solution when $\bar{\mathbf{M}} = \mathbf{M}$. Thus, to lowest order

$$\epsilon^T_{\alpha\beta} = K(2\pi r)^{-1/2}\tilde{\epsilon}^T_{\alpha\beta}(\theta) \tag{A9}$$

where

$$\tilde{\epsilon}^T_{\alpha\beta}(\theta) = (\bar{M}_{\alpha\beta\kappa\gamma} - M_{\alpha\beta\kappa\gamma})\tilde{\sigma}_{\kappa\gamma}(\theta). \tag{A10}$$

The stress intensity K^0_{tip}, in (A8) is the amplitude of the near-tip singular fields within the inner circular region.

Next, (A10) is substituted into (A8) and the integration with respect to r is performed with the result

$$\frac{K^0_{tip}}{K} = 1 + \frac{1}{4\pi}\frac{E}{(1-\nu^2)} \times \int_0^\pi \{\ln[R(\theta)] - \ln\rho\} h_{\alpha\beta}(\theta)\tilde{\epsilon}^T_{\alpha\beta}(\theta)\,d\theta. \tag{A11}$$

A straightforward evaluation of $h_{\alpha\beta}\tilde{\epsilon}^T_{\alpha\beta}$ using the well-known expressions for $\tilde{\sigma}_{\alpha\beta}$ gives

$$\frac{E}{(1-\nu^2)} h_{\alpha\beta}\tilde{\epsilon}^T_{\alpha\beta} = \tfrac{1}{8}\delta_1(11\cos\theta + 8\cos 2\theta - 3\cos 3\theta) - 2\delta_2(\cos\theta + \cos 2\theta). \tag{A12}$$

It is here that the moduli parameters δ_1 and δ_2 defined by (3.6) and (3.7) emerge naturally. Since

$$\int_0^\pi h_{\alpha\beta}\tilde{\epsilon}^T_{\alpha\beta}\,d\theta = 0,$$

it follows that

$$K^0_{tip}/K = 1 + k_1\delta_1 + k_2\delta_2 \tag{A13}$$

where k_1 and k_2 are defined in (3.10) and (3.11). It is essential to interpret K^0_{tip} as the intensity factor of the singular fields within the inner circular core with moduli (E, ν) and *not* the desired factor K_{tip}. Condition (A3) on the transformation strains excludes the identification of K^0_{tip} with K_{tip} and thereby motivates the two-step solution procedure employed here. Equation (A13) implies that K^0_{tip}/K is independent of the radius ρ of the inner circular core, to lowest order in the δ's.

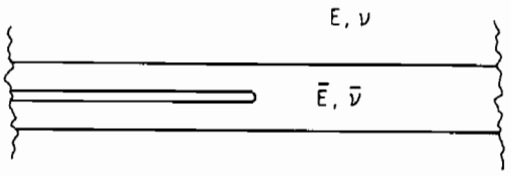

Fig. 11. Special geometry used to infer solution to auxiliary problem *B*.

To generate the solution to *auxiliary problem B*, we exploit a special region A_c for which K_{tip}/K is known. Then by evaluating K^0_{tip}/K for this region, we can "back-out" the desired universal result K^0_{tip}/K_{tip} for problem *B* using (A5).

The special region A_c is the infinite strip with a centered semi-infinite crack shown in Fig. 11. Either a simple energy argument or application of the *J*-integral implies that (5.10) holds exactly for this problem. By (3.14), this gives

$$K_{tip}/K = [1 + \delta_1 - \delta_2]^{-1/2} \tag{A14}$$

which is not limited to lowest order.

The integrals in the definitions of k_1 and k_2 are easily evaluated for this geometry giving for problem *A*

$$K^0_{tip}/K = 1 + \tfrac{1}{8}\delta_1 - \tfrac{1}{4}\delta_2. \tag{A15}$$

Then, combining (A14) and (A15) according to (A5), one immediately obtains the lowest order result for problem *B*

$$K^0_{tip}/K_{tip} = 1 + \tfrac{5}{8}\delta_1 - \tfrac{3}{4}\delta_2. \tag{A16}$$

Finally, the general result (3.9) for arbitrarily shaped regions follows by combining (A13) and (A16) according to (A5).

K_{tip} *for Circular Regions* A_c

An extensive study of the problem posed in Fig. 2 (with $\theta^T = 0$) has been given in [14] for the case of circular regions A_c centered at the tip of the semi-infinite crack. Techniques from complex variable elasticity together with numerical computation were used to compute K_{tip}/K for arbitrary differences in the sets of moduli. We have independently checked both the analysis and the numerical calculations in [14], finding our results to be in complete agreement with those in [14]. (The fact that the solution could be collapsed to a dependence on just two moduli variables, such as δ_1 and δ_2, was not exploited in [14].)

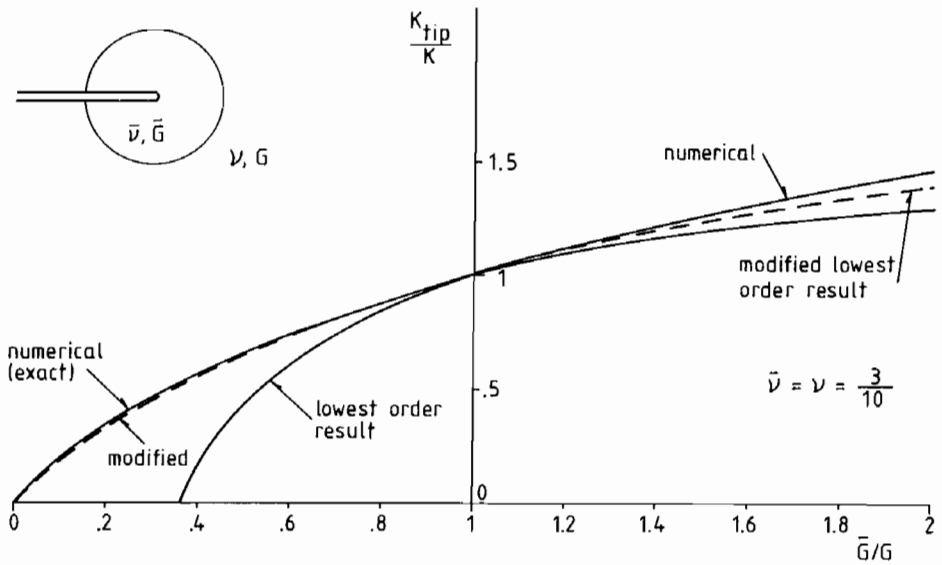

Fig. 12. A comparison of selected results for circular micro-crack zone.

A numerical example is shown in Fig. 12. In this example $\bar{\nu} = \nu = 3/10$ and the ratio of shear moduli is varied. Included in Fig. 12 is the lowest order result for the circular region from (3.9)

$$K_{tip}/K = 1 - \tfrac{5}{8}\delta_1 + \tfrac{3}{4}\delta_2 \doteq 1 - \tfrac{4}{7}(G/\bar{G} - 1)(\nu = \bar{\nu} = 3/10). \quad \text{(A17)}$$

The example again illustrates that lowest order results capture trends but are not numerically accurate when the moduli differences become large. The *modified lowest order formula* (6.1) gives

$$K_{tip}/K = [1 + (4/7)(G/\bar{G} - 1)]^{-1} \quad \text{(A18)}$$

which is seen in Fig. 12 to have a much greater range of accuracy. Similarly, the modified lowest order result for the infinite strip problem, whose exact result is given by (A14), has a much improved range of accuracy.

Nonuniform Micro-crack Distribution—Stationary Crack

In the lowest order calculation the unperturbed stress field (3.2) can be used to determine the distribution of the micro-crack density. Using the nucleation criterion based on the mean stress in Fig. 5, we will illustrate the fact that the lowest order result for the contribution to K_{tip} due to the reduction in moduli is independent of the details of the transition from uncracked to saturated cracking and is the same as the result calculated using the simplified criterion. That is, the result is the same as that calculated using the uniform moduli of the saturated state everywhere in A_c. This feature was observed to hold without limit to lowest order in (5.4) and (5.14) for the two special materials for which the J-integral permitted the near-tip and remote fields to be linked.

From (3.2), the mean stress is

$$\sigma_m = \tfrac{2}{3}(1 + \nu)K(2\pi r)^{-1/2}\cos(\theta/2). \quad \text{(A19)}$$

Based on the micro-cracking relation in Fig. 5(a), the inner and outer boundaries of Fig. 4 are obtained by setting σ_m to be σ_m^s and σ_m^c, respectively. It is immediately seen that $R_s(\theta) = (\sigma_m^c/\sigma_m^s)^2 R(\theta)$. Moreover, the level of micro-cracking scales with $r/R(\theta)$. Thus, the micro-crack distribution fits exactly into the assumptions of Section 3.2, to lowest order. To see that K_{tip} depends only on δ_1^s and δ_2^s, as claimed in Section 3.2, repeat the steps leading to (A11) taking the inner core radius ρ fully within the saturated zone and noting that δ_1 and δ_2 depend on position as in (3.17). The result then follows directly when one notes that the contribution to K_{tip}^0 from the transition region, $R_s(\theta) \lesssim r \lesssim R(\theta)$, is zero. The conclusion also holds for other nucleation criteria such as that based on the maximum principal stress. It should be noted that the conclusion does not apply to the growing crack. The above technique can be applied to obtain lowest order results for the growing crack when the micro-crack distribution is non-uniform.